Detachment in Fusion Plasmas with Symmetry Breaking Magnetic Perturbation Fields

H. Frerichs* and O. Schmitz
Department of Engineering Physics, University of Wisconsin, Madison, Wisconsin 53706, USA

X. Bonnin and A. Loarte
ITER Organization, Route de Vinon-sur-Verdon, CS 90 046, 13067 St. Paul Lez Durance Cedex, France

Y. Feng
Max-Planck-Institut für Plasmaphysik, Association EURATOM-IPP, 17491 Greifswald, Germany

L. Li
College of Science, Donghua University, Shanghai 201620, People's Republic of China

Y. Q. Liu
General Atomics, P.O. Box 85608, San Diego, California 92186-5608, USA

D. Reiter
Institute for Laser and Plasma Physics, Heinrich-Heine-University, D-40225 Duesseldorf, Germany

(Received 12 September 2019; revised 24 June 2020; accepted 9 September 2020; published 9 October 2020)

Power exhaust from the bulk plasma is significantly altered by symmetry breaking magnetic perturbation fields, because these create direct connections (perturbed field lines) from the confined high temperature plasma to solid surfaces. The same amount of power is distributed among those new exhaust channels as for a symmetric magnetic configuration, which reduces the local upstream heat flux flowing down the perturbed field lines, thereby making access to detachment easier (i.e., at lower upstream density) for the divertor plasma near the location corresponding to the symmetric magnetic separatrix. However, the divertor plasma regions with connection to the bulk plasma are extended nonaxisymmetrically further outside, where significant heat loads occur, unlike in the symmetric configuration. The temperature remains high at those locations, which reduces the divertor plasma dissipation capacity, making the mitigation of heat loads more difficult to achieve.

DOI: 10.1103/PhysRevLett.125.155001

Developing a viable solution for the plasma boundary remains a grand challenge for magnetically confined fusion energy production, because it involves the interplay of a number of fundamentally different, but individually highly nonlinear processes. The neutral particles in the surrounding of the plasma—and, in particular, the ones originating in the neutralization and reemission process of plasma ions striking material surfaces (also known as recycling)—provide an energy sink to the boundary plasma. This sink can be highly localized with a strongly varying energy loss rate depending on the local plasma temperature. When the plasma density is increased to levels relevant for later high fusion energy gain, the plasma temperature in front of material surfaces can be reduced, thereby rapidly crossing through a regime in which the energy loss rates change over several orders of magnitude for comparably small (several eV) changes in the plasma temperature. This mechanism is advantageous, because the conductive energy outflux is mostly exhausted through interaction with neutral particles and/or seeded impurities, while the remaining energy and also particle flux to dedicated material surfaces (divertor targets) is significantly reduced. This nonlinear energy loss scenario is called detachment [1,2]. In ITER (the next step magnetically confined fusion energy experiment based on the axisymmetric tokamak concept [3]), it has to be combined with the challenge of suppressing a typical class of pressure gradient and current density driven edge instabilities, the edge localized modes (ELMs) [4], which are naturally associated with standard high confinement (H-mode) operation [5]. ELM control may be achieved by introducing three-dimensional (3D), chaotic magnetic field structures from small amplitude, symmetry breaking external magnetic perturbation (MP) fields [6–8]. In this Letter, we extend an earlier exploration of the linear recycling regime with MP fields [9] into the nonlinear regime and evaluate for the first time the impact of MP fields on detachment in ITER (which is the foreseen divertor operational regime). We highlight changes in divertor operation resulting from connecting the bulk plasma to strike locations in both the nominal near and far scrape-off

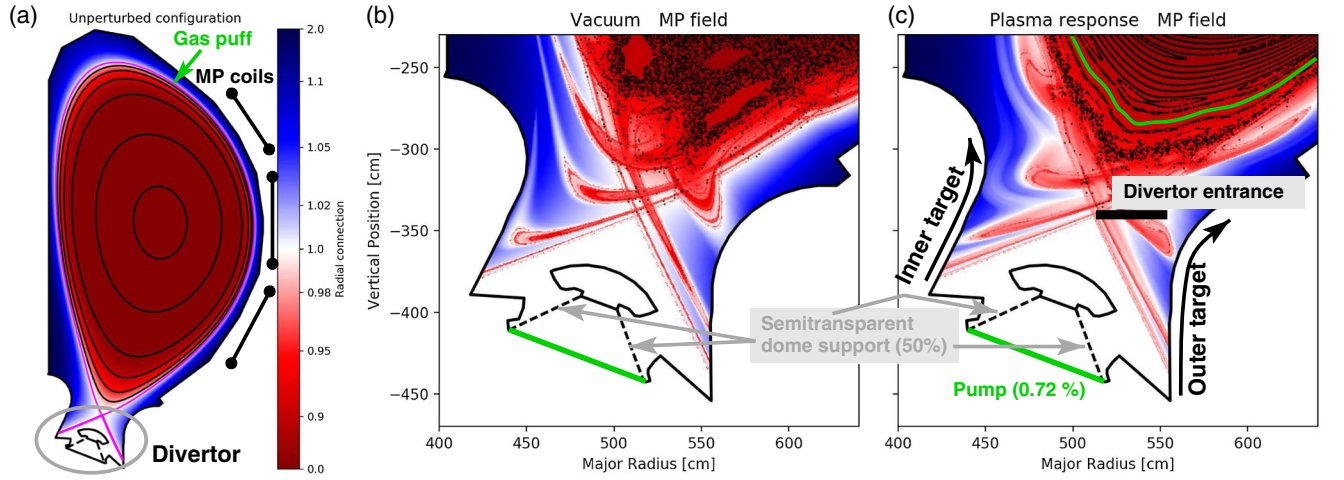

FIG. 1. (a) Magnetic geometry of an unperturbed (axisymmetric) configuration $\mathbf{B}_{\mathrm{equi}}$ anticipated for the PFPO phase in ITER running at low power (30 MW) and reduced field and current (1.8 T/5 MA). (b) Perturbed configuration $\mathbf{B}_{\mathrm{equi}} + \mathbf{B}_{\mathrm{MP}}$ with external MP field powered by 30 kA coil current in $n = 3$ toroidal mode number configuration and phasing optimized for ELM control. (c) Perturbed configuration $\mathbf{B}_{\mathrm{equi}} + \mathbf{B}_{\mathrm{MP}} + \mathbf{B}_{\mathrm{plasma}}$ including the internal response to the MP field calculated by MARS-F. A Poincaré map is shown by black dots, and the radial connection $\mathcal{R}$ (evaluated as the minimum of the normalized poloidal magnetic flux Ψ_N that a perturbed field line encounters) is shown in color.

layer (SOL). For this we focus on the initial H-mode plasmas to be obtained in the prefusion plasma operation (PFPO) phase with up to 30 MW of additional heating, for which no active measures to mitigate divertor head loads are expected to be required. We leave the added complexity of supplementing and fine-tuning edge radiation by impurity seeding at the $Q = 10$ heating power (50 MW of additional heating plus 100 MW of alpha heating) for a later, more detailed analysis.

The unperturbed (axisymmetric) configuration $\mathbf{B}_{\mathrm{equi}}$ is shown in Fig. 1(a) for reference: the bulk plasma with closed, nested magnetic flux surfaces Ψ_N is disconnected by a magnetic separatrix (purple) from the scrape-off layer, where field lines are diverted onto dedicated targets. During application of small perturbations $\mathbf{B}_{\mathrm{MP}}$ a chaotic layer is formed by overlap of neighboring magnetic island chains that appear where $\mathbf{B}_{\mathrm{MP}} \cdot \nabla\Psi_N$ is resonant with the field line pitch angle of the helical $\mathbf{B}_{\mathrm{equi}}$. Furthermore, the magnetic separatrix splits into two distinct (forward and backward) branches of helical lobes, which are determined by the nonresonant components [10] (see, e.g., Fig. 1 in Ref. [11]). This structure is not specific to magnetic confinement fusion plasmas, but is a rather well-known phenomenon in nonlinear dynamics in perturbed systems with a hyperbolic fixed point [12,13]. Field lines from the chaotic layer can escape to the divertor targets guided by this perturbed nonaxisymmetric separatrix. The magnetic geometry can be modified by an internal response $\mathbf{B}_{\mathrm{plasma}}$ of the plasma to the external $\mathbf{B}_{\mathrm{MP}}$ [see, e.g., Ref. [14] for a brief review of present magnetohydrodynamics (MHD) models for plasma response]. In this Letter, we take into account such a response by applying MARS-F [15]: a linearized, resistive single fluid MHD model.

In the following, we focus on MP application in ITER with toroidal mode number $n = 3$, and select one specific case for which the phasing between the three rows of window-frame type coils has been optimized for ELM control (by maximizing the kink-peeling amplification near the separatrix) [16]. We find that the plasma response combines strong screening of the resonances in the bulk plasma with an amplification of mostly nonresonant components at the plasma edge just inside the separatrix of the symmetric configuration. The former is reflected in Poincaré plots, which show that the resulting chaotic domain in Fig. 1(c) with $\mathbf{B}_{\mathrm{plasma}}$ included is smaller than in Fig. 1(b), where $\mathbf{B}_{\mathrm{plasma}}$ has been neglected. The latter is reflected in the colored contours, which show that the radial extension of the helical lobe structure of the perturbed separatrix is similar in both cases and does not shrink as expected from screening-only models (which seem to fit well for the Axially Symmetric Divertor Experiment Upgrade [17]). It should be noted that this model (MARS-F) is capable of quantitatively reproducing the measured 3D plasma response field in DIII-D plasmas and predicting the optimal resonant magnetic perturbation coil current phasing in Mega Ampere Spherical Tokamak (MAST) (see Ref. [14] and references therein) even though MP penetration is a highly nonlinear process [18]. Also, it should be noted that pedestal conditions in ITER and present day machines are not the same, which may be responsible for different levels of amplification.

Fluid models are commonly applied for characterization of the plasma boundary by local parameters such as the plasma density n, flow velocity along field lines $u_{\|}$, and temperature T (often split into an electron and ion component T_e, T_i). In steady state, fluid equations are of the form

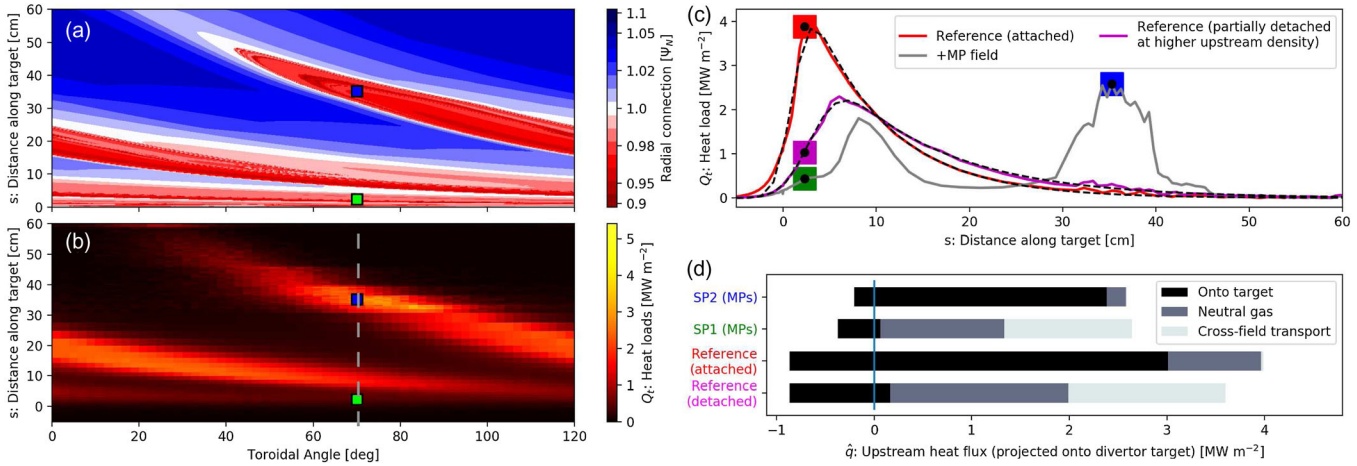

FIG. 2. (a) Magnetic footprint at the outer divertor target in Fig. 1(c), characterized by the radial connection $\mathcal{R}$ of field lines. (b) Corresponding heat loads Q_t as calculated by EMC3-EIRENE for $\Gamma_{\text{gas puff}} = 3 \times 10^{22}$ s^{-1}. Profiles of Q_t at the highlighted toroidal position are shown in (c) in comparison to the (unperturbed) reference configuration with a fit (dashed line) to Eq. (2) in Ref. [19]. The distance along the target is measured from the symmetric magnetic separatrix strike point (SP). (d) Power balance on field line at selected strike locations: the upstream heat flux $\hat{q}$ is either deposited on the target (black), dissipated from interaction with neutral gas (dark gray), or spread through cross-field transport (light gray). The negative extension of the black bars indicate the contribution of surface recombination to Q_t, which is not provided by $\hat{q}$.

$$\nabla \cdot \mathbf{\Gamma} = S_p, \tag{1}$$

$$\nabla \cdot \boldsymbol{\mathcal{M}} = -\nabla_\parallel p + S_m, \tag{2}$$

$$\nabla \cdot \mathbf{q} = S_e, \tag{3}$$

where particle flux $\mathbf{\Gamma}$ is balanced by sources and sinks S_p (from ionization of neutral particles or recombination). Momentum flux $\boldsymbol{\mathcal{M}}$ along field lines is driven by a gradient of the plasma pressure $p = n(T_e + T_i)$ and is balanced by momentum losses S_m (largely from charge exchange with neutral particles), and heat flux $\mathbf{q}$ is balanced by energy losses S_e (from ionization and molecular dissociation, including excitation and subsequent photon emission). Unlike common fluids, however, transport is extremely anisotropic in plasmas, and transport along field lines exceeds cross-field transport by several orders of magnitude. The former is represented reasonably well within the classical closure of the fluid equations for collisional plasmas [20], which results in conductive heat fluxes

$$q_\parallel^{(\text{cond})} = -\kappa_\parallel \nabla_\parallel T, \qquad \kappa_\parallel \sim T^{5/2} \tag{4}$$

with strong nonlinear conductivity $\kappa_\parallel$. The latter is less well understood and is in macroscopic models of the plasma boundary commonly referred to as "anomalous transpor" to be described by a diffusion ansatz with free model parameters. The design of the ITER divertor has been guided by a two-dimensional (axisymmetric) implementation of (1)–(3), namely, SOLPS [21], but whether detachment remains compatible with MP application has not been addressed. This requires a 3D model instead (such as EMC3-EIRENE [22]). After recent improvements regarding stabilization of the iterative approximation of the nonlinear plasma boundary for low divertor temperatures, numerical access to detached plasmas in nonaxisymmetric tokamak configurations is now possible for the first time [23]. Simulations are performed based on a standard set of model parameters for cross-field diffusion ($D_\perp = 0.3$ and $\chi_\perp = 1$ m^2 s^{-1}), which results in an upstream (near-SOL) power falloff length $\lambda_q \approx 3$–4 mm consistent with Fig. 4 in Ref. [24]. Presently, $\mathbf{E} \times \mathbf{B}$ drifts are not included in the 3D model (and were omitted in most 2D simulations guiding the ITER divertor design as well). Steady state particle balance is maintained between gas puffing ($\Gamma_{\text{gas puff}}$), fueling at the core boundary ($\Gamma_{\text{core}} = 5 \times 10^{20}$ s^{-1}) just inside the last closed flux surface, and pumping from below the dome with a probability of 0.72% (locations are indicated in green in Fig. 1). The edge heating power is set to $P_{\text{SOL}} = 30$ MW for the PFPO phase.

A key role for the divertor state is the boundary condition for the plasma due to interaction with solid surfaces. Macroscopic plasma models do not resolve the thin plasma sheath in front of solid surfaces, but rather link the incoming heat flux q_t to the particle flux Γ_t through a sheath heat transmission coefficient $\gamma \sim 7$ and the plasma temperature T_t,

$$q_t = \gamma T_t \Gamma_t, \qquad Q_t = q_t + \varepsilon \Gamma_t, \tag{5}$$

thereby eliminating 1 degree of freedom between the three parameters Γ_t, T_t, and q_t. The resulting heat load on the target Q_t includes the deposited energy $\varepsilon \approx 13.6 + 2$ eV from recombination of the incident ion flux into atoms and

further into molecules. Power dissipation in the divertor can be evaluated following the two point formatting (Sec. 11 in Ref. [2]) by mapping the heat flux $q_{u\parallel}$ at the divertor entrance upstream (evaluated just above the X point) along field lines to the target,

$$1 - f_{\mathrm{cool}} = \frac{q_{t\parallel}}{B_t}\frac{B_u}{q_{u\parallel}} = q_t \Bigg(\underbrace{q_{u\parallel}\frac{B_t}{B_u}\sin\theta}_{=\hat{q}} \Bigg)^{-1}, \qquad (6)$$

where $q_t = q_{t\parallel}\sin\theta$ accounts for the oblique incident of field lines on the target.

In comparing Figs. 2(a) and 2(b), one can see that heat loads appear where perturbed field lines connect into the bulk plasma. Figure 2(c) shows that the unperturbed configuration (red) is still attached in a simulation with comparable upstream density $n_u \approx 1.6$–1.7×10^{19} m^{-3} (see also Fig. 3) and that the profile matches the archetypal shape of a convolution of an exponential with a Gaussian function (black dashed line, obtained by fitting simulation results to Eq. (2) in Ref. [19]). The corresponding power balance in Fig. 2(d) shows that most of the upstream heat flux $\hat{q}$ is indeed deposited on the target, while only a minor part is dissipated through interaction with neutral gas. Integrated over the near SOL (up to $s \approx 10$ cm), 65% of the power entering the divertor upstream is still deposited on the target. A partially detached state (purple) at higher upstream density is shown for comparison, and here the majority of $\hat{q}$ is either dissipated or spread through cross-field transport [note that the profile shape in Fig. 2(c) is still represented by Eq. (2) in Ref. [19], but that it is shifted further outward with respect to the attached case].

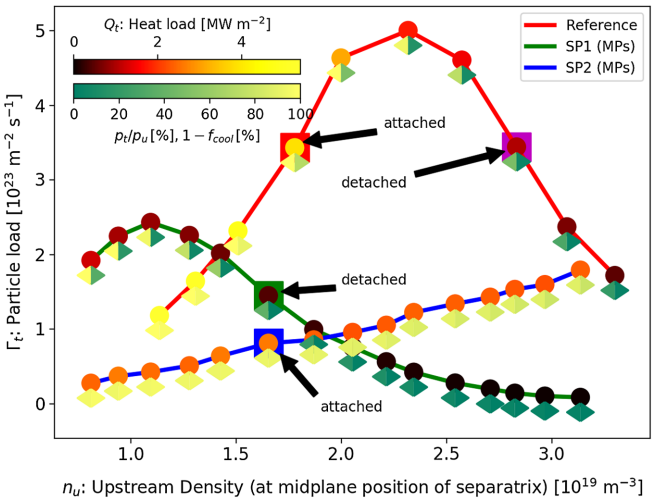

FIG. 3. Characteristic curves of the divertor state with and without MP field. Corresponding heat loads Q_t are shown by colored circles, while pressure (◀) and power balances (▶) are shown by colored symbols below. Results from Figs. 2(c) and 2(d) are highlighted by colored boxes and are annotated with arrows.

In the following, we compare divertor performance at two strike points with magnetic connection to the bulk plasma when MP fields are applied: SP1 located in the former near SOL (highlighted in green in Fig. 2) and SP2 located in the former far SOL (highlighted in blue). The reference for SP1 is highlighted red in Fig. 2(c), while the reference divertor state for SP2 is irrelevant because $\hat{q}$ is negligible here. The power balance in Fig. 2(d) shows that SP1 is already detached, similar to the detached reference case without MP fields at higher n_u. Integrated over the near SOL, only 14% of the upstream influx is deposited on the target. SP2, however, remains attached, with significant upstream heat flux $\hat{q}$ being deposited onto the divertor target without dissipation.

A density scan (by varying $\Gamma_{\mathrm{gaspuff}}$) has been performed to explore the impact of MP fields on the transition to detachment, and the resulting characteristic curves for Γ_t are shown in Fig. 3. The unperturbed SP (red line) exhibits the typical behavior: particle loads are initially increasing and then come to a roll-over point (detachment transition) once power losses (f_{cool}) set in. After the roll-over, the detached state is characterized by both pressure and power losses between the divertor entrance and the target. The same behavior is found with MP field at SP1 (green line), except roll-over occurs already at a lower density with lower peak particle load. This is completely different at SP2 (blue line), which remains attached at high T_t, and the resulting high Q_t ultimately exceeds that of the unperturbed reference once the latter detaches. The higher T_t at SP2 follows from (1) higher upstream temperature T_u due to a deeper connection into the bulk plasma evident from Fig. 2(a), and (2) a shorter connection length to the bulk plasma (resulting from field lines passing the X point at a greater distance) causing a tighter coupling between T_u and T_t according to (4).

This is possibly reinforced by the divertor target geometry, which favors reflection of recycled neutral particles away from the far SOL, thereby reducing their contributions to dissipation here and keeping SP2 in a low-recycling state (unlike in open divertor configurations such as in DIII-D, where the opposite trend is observed [25,26]). Power losses are in fact negligible at SP2 ($f_{\mathrm{cool}} \approx 0$, see Fig. 3), thereby leading to a linear decrease of T_t with the inverse of Γ_t as long as $\hat{q}$ (and thus q_t) remains constant. A moderate increase of q_t may even be found at SP2 from redirecting power exhaust from the bulk plasma during the detachment transition at SP1. The presence of such a regime was identified by experimental results at the Experimental Advanced Superconducting Tokamak [27]. It is important to note that even higher T_u is expected for the full power burning plasma phase, which implies even more severe conditions at the far-SOL strike locations connected to the bulk plasma and thus raises concerns regarding the magnitude of the local power fluxes and divertor lifetime (tungsten sputtering). To address these concerns, the

ITER ELM control coil system is designed to apply rotating MP fields at frequencies of several hertz [28]; however, it is desirable to use this capability only when needed to minimize fatigue lifetime consumption of these coils. To determine when such capability will be needed, it is necessary to further develop and apply high fidelity models for the perturbed plasma boundary (including effects of plasma response, impurity seeding, $\mathbf{E} \times \mathbf{B}$ drifts, etc.) and to further validate their predictions experimentally.

Conclusions.—Power exhaust from the bulk plasma is significantly altered by MP fields due to direct connections (i.e., transport along field lines) to both near- and far-SOL strike locations on the divertor targets. The same amount of P_{SOL} is distributed among those exhaust channels, leading to lower near-SOL $\hat{q}$ at comparable upstream densities and thereby making detachment transition easier at these locations. Conversely, $\hat{q}$ to the far SOL is significantly increased, and temperatures remain higher due to the more direct link to the bulk plasma. Thus, unlike in the reference configuration, a later detachment of the far SOL implies significant heat loads to those locations that are more difficult to mitigate on the divertor targets at ITER.

This work was supported by the U.S. Department of Energy under Awards No. DE-SC0020357, No. DE-SC00013911, and No. DE-SC0020284, and by the College of Engineering at the University of Wisconsin–Madison. This work was done under the auspices of the ITER Scientist Fellow Network. The views and opinions expressed herein do not necessarily reflect those of the ITER Organization. Computer simulations have been performed at the UW-Madison Center for High Throughput Computing (CHTC) and at the ITER General Purpose Computing (GPC) cluster.

*hfrerichs@wisc.edu

[1] S. I. Krasheninnikov and A. S. Kukushkin, Physics of ultimate detachment of a tokamak divertor plasma, J. Plasma Phys. **83**, 155830501 (2017).

[2] P. C. Stangeby, Basic physical processes and reduced models for plasma detachment, Plasma Phys. Controlled Fusion **60**, 044022 (2018).

[3] J. Wesson, *Tokamaks*, 4th ed., International Series of Monographs on Physics Vol. 149 (Oxford University Press, New York, 2011).

[4] H. Zohm, Edge localized modes (ELMs), Plasma Phys. Controlled Fusion **38**, 105 (1996).

[5] ITER Physics Expert Group on Confinement and Transport *et al.*, Chapter 2: Plasma confinement and transport, Nucl. Fusion **39**, 2175 (1999).

[6] T. E. Evans *et al.*, Suppression of Large Edge-Localized Modes in High-Confinement DIII-D Plasmas with a Stochastic Magnetic Boundary, Phys. Rev. Lett. **92**, 235003 (2004).

[7] Y. Liang *et al.*, Active Control of Type-I Edge-Localized Modes with $n = 1$ Perturbation Fields in the JET Tokamak, Phys. Rev. Lett. **98**, 265004 (2007).

[8] W. Suttrop, T. Eich, J. C. Fuchs, S. Günter, A. Janzer, A. Herrmann, A. Kallenbach, P. T. Lang, T. Lunt, M. Maraschek, R. M. McDermott, A. Mlynek, T. Pütterich, M. Rott, T. Vierle, E. Wolfrum, Q. Yu, I. Zammuto, H. Zohm, and ASDEX Upgrade Team, First Observation of Edge Localized Modes Mitigation with Resonant and Nonresonant Magnetic Perturbations in ASDEX Upgrade, Phys. Rev. Lett. **106**, 225004 (2011).

[9] O. Schmitz, M. Becoulet, P. Cahyna, T. E. Evans, Y. Feng, H. Frerichs, A. Loarte, R. A. Pitts, D. Reiser, M. E. Fenstermacher, D. Harting, A. Kirschner, A. Kukushkin, T. Lunt, G. Saibene, D. Reiter, U. Samm, and S. Wiesen, Three-dimensional modeling of plasma edge transport and divertor fluxes during application of resonant magnetic perturbations on ITER, Nucl. Fusion **56**, 066008 (2016).

[10] T. E. Evans, R. K. W. Roeder, J. A. Carter, and B. I. Rapoport, Homoclinic tangles, bifurcations and edge stochasticity in diverted tokamaks, Contrib. Plasma Phys. **44**, 235 (2004).

[11] H. Frerichs, O. Schmitz, T. Evans, Y. Feng, and D. Reiter, The pattern of parallel edge plasma flows due to pressure gradients, recycling, and resonant magnetic perturbations in DIII-D, Phys. Plasmas **22**, 072508 (2015).

[12] J. Guckenheimer and P. Holmes, Nonlinear oscillations, dynamical systems, and bifurcations of vector fields, Appl. Math. Sci. **42**, 45 (1983).

[13] A. J. Lichtenberg and M. A. Lieberman, *Regular and Chaotic Dynamics*, 2nd ed., Applied Mathematical Sciences Vol. 38 (Springer-Verlag, New York, 1992).

[14] Y. Liu, C. J. Ham, A. Kirk, L. Li, A. Loarte, D. A. Ryan, Y. Sun, W. Suttrop, X. Yang, and L. Zhou, ELM control with RMP: Plasma response models and the role of edge peeling response, Plasma Phys. Controlled Fusion **58**, 114005 (2016).

[15] Y. Q. Liu, A. Bondeson, C. M. Fransson, B. Lennartson, and C. Breitholtz, Feedback stabilization of nonaxisymmetric resistive wall modes in tokamaks. I. Electromagnetic model, Phys. Plasmas **7**, 3681 (2000).

[16] L. Li, Y. Q. Liu, N. Wang, A. Kirk, H. R. Koslowski, Y. Liang, A. Loarte, D. Ryan, and F. C. Zhong, Toroidal modeling of plasma response to RMP fields in ITER, Plasma Phys. Controlled Fusion **59**, 044005 (2017).

[17] D. Brida, T. Lunt, M. Wischmeier, M. Bernert, D. Carralero, M. Faitsch, Y. Feng, T. Sehmer, B. Sieglin, W. Suttrop, and E. Wolfrum, The ASDEX Upgrade Team, and The MST1 Team, Heat flux pattern in detached L-modes and ELM mitigated H-modes with rotating magnetic perturbations in ASDEX Upgrade, Nucl. Fusion **57**, 116006 (2017).

[18] F. Orain, M. Hoelzl, F. Mink, M. Willensdorfer, M. Bécoulet, M. Dunne, S. Günter, G. Huijsmans, K. Lackner, S. Pamela, W. Suttrop, E. Viezzer, and ASDEX Upgrade Team, and EUROfusion MST1 Team, Non-linear modeling of the threshold between ELM mitigation and ELM suppression by resonant magnetic perturbations in ASDEX upgrade, Phys. Plasmas **26**, 042503 (2019).

[19] T. Eich, B. Sieglin, A. Scarabosio, W. Fundamenski, R. J. Goldston, A. Herrmann, and ASDEX Upgrade Team, Inter-ELM Power Decay Length for JETand ASDEX Upgrade:

Measurement and Comparison with Heuristic Drift-Based Model, Phys. Rev. Lett. **107**, 215001 (2011).

[20] S. I. Braginskii, Transport processes in a plasma, Rev. Plasma Phys. **1**, 205 (1965).

[21] A. S. Kukushkin, H. D. Pacher, V. Kotov, G. W. Pacher, and D. Reiter, Finalizing the ITER divertor design: The key role of SOLPS modeling, Fusion Eng. Des. **86**, 2865 (2011).

[22] Y. Feng, H. Frerichs, M. Kobayashi, and D. Reiter, Monte-Carlo fluid approaches to detached plasmas in non-axisymmetric divertor configurations, Plasma Phys. Controlled Fusion **59**, 034006 (2017).

[23] H. Frerichs, X. Bonnin, Y. Feng, A. Loarte, R. A. Pitts, D. Reiter, and O. Schmitz, Stabilization of EMC3-EIRENE for detachment conditions and comparison to SOLPS-ITER, Nucl. Mater. Energy **18**, 62 (2019).

[24] R. A. Pitts, X. Bonnin, F. Escourbiac, H. Frerichs, J. P. Gunn, T. Hirai, A. S. Kukushkin, E. Kaveeva, M. A. Miller, D. Moulton, V. Rozhansky, I. Senichenkov, E. Sytova, O. Schmitz, P. C. Stangeby, G. De Temmerman, I. Veselova, and S. Wiesen, Physics basis for the first ITER tungsten divertor, Nucl. Mater. Energy **20**, 100696 (2019).

[25] H. Frerichs, O. Schmitz, D. Reiter, T. E. Evans, and Y. Feng, Striation pattern of target particle and heat fluxes in three dimensional simulations for DIII-D, Phys. Plasmas **21**, 020702 (2014).

[26] A. R. Briesemeister, J.-W. Ahn, J. M. Canik, M. E. Fenstermacher, H. Frerichs, C. J. Lasnier, J. D. Lore, A. W. Leonard, M. A. Makowski, A. G. McLean, W. H. Meyer, O. Schmitz, M. W. Shafer, E. A. Unterberg, H. Q. Wang, and J. G. Watkins, Changes in divertor conditions in response to changing core density with RMPs, Nucl. Fusion **57**, 076038 (2017).

[27] J. Li, H. Y. Guo, B. N. Wan, X. Z. Gong, Y. F. Liang, G. S. Xu, K. F. Gan, J. S. Hu, H. Q. Wang, L. Wang, L. Zeng, Y. P. Zhao, P. Denner, G. L. Jackson, A. Loarte, R. Maingi, J. E. Menard, M. Rack, and X. L. Zou, A long-pulse high-confinement plasma regime in the experimental advanced superconducting Tokamak, Nat. Phys. **9**, 817 (2013).

[28] A. Loarte *et al.*, Progress on the application of ELM control schemes to ITER scenarios from the non-active phase to DT operation, Nucl. Fusion **54**, 033007 (2014).